Development of a fluid bed granulation process control strategy based on real-time process and product measurements

Anneleen Burggraeve[a], Ana F.T. Silva[a], Tom Van Den Kerkhof[b], Mario Hellings[b], Chris Vervaet[c], Jean Paul Remon[c], Yvan Vander Heyden[d], Thomas De Beer[a*]

[a]Laboratory of Pharmaceutical Process Analytical Technology, Faculty of Pharmaceutical Sciences, Ghent University, Belgium

[b]Johnson & Johnson Pharmaceutical Research and Development, Analytical Development, Beerse, Belgium

[c]Laboratory of Pharmaceutical Technology, Faculty of Pharmaceutical Sciences, Ghent University, Belgium

[d]Department of Analytical Chemistry and Pharmaceutical Technology, Faculty of Medicine and Pharmacy, Vrije Universiteit Brussel –VUB, Belgium

[*]Corresponding author:

Thomas De Beer

Harelbekestraat 72

B-9000 Ghent

Belgium

Tel: +32 9 264 80 97

Fax: +32 9 222 82 36

Email: thomas.debeer@ugent.be

Abstract

This article describes the results of three case studies conducted consecutively, in order to develop a process control strategy for a top-spray fluid bed granulation process. The use of several real-time particle size *(i.e., spatial filter velocimetry and focused beam reflectance measurement)* and moisture *(i.e., near infrared (NIR) and Lighthouse near infrared spectroscopy)* analyzers was examined. A feed-forward process control method was developed, where in-line collected granulation information during the process spraying phase was used to determine the optimum drying temperature of the consecutive drying phase. Via real-time monitoring of process *(i.e., spraying temperature and spray rate)* and product *(i.e., granule size distribution and moisture)* parameters during the spraying period, the batch bulk density was predicted at the end of the spraying cycle, using a PLS model. When this predicted bulk density was not meeting the desired value, the developed control method allowed the calculation of an adjusted drying temperature leading to the desired batch bulk density at the end of the granulation process. Besides the development of the feed-forward control strategy, a quantitative PLS model for in-line moisture content prediction of the granulated end product was built using the NIR data.

Key words

Fluid bed granulation – NIR spectroscopy – spatial filter velocimetry (SFV) – focused beam reflectance measurement (FBRM) – in-line monitoring – process control

1. Introduction

Fluid bed granulation has extensively been used in the pharmaceutical industry since Wurster proposed the agglomeration process for pharmaceutical applications over five decades ago [1, 2]. Top-spray fluid bed granulation entails the suspension of powder particles in an air stream and spraying a binder liquid from the top down (counter-current to the fluidizing air) onto the fluidized bed. In that way, moistened particles collide with each other, agglomerate and form granules. After spraying the required amount of granulation liquid (spraying phase), the product is dried inside the fluid bed granulator until a pre-set exhaust air temperature is achieved corresponding to the desired moisture level (drying phase). Similar to all other wet (or dry) granulation processing techniques, the main objectives of fluid bed granulation are to improve the flow characteristics and compactibility of a powder mixture, to decrease dustiness and/or to prevent mixture segregation. It is a complex process as many interrelated parameters influence the granule properties and consequently the quality of the resulting tablets.

Traditionally in pharmaceutical batch manufacturing, the critical quality attributes of the end product are assessed via off-line laboratory testing. Depending on the outcome of these tests, the batches are labeled as in- or out-of-specification products and are released or discarded. A more efficient way of operating consists of in-process quality assessments based on timely measurements, offering real-time quality evaluation of intermediate and end products. The Process Analytical Technology (PAT) framework initiated by the Food and Drug Administration (FDA) encourages to move from off-line laboratory tests to timely measurements executed directly in or near the process environment [3]. Off-line measurements should be replaced by at-line, on-line or in-line measurements.

The control of fluid bed granulation processes conventionally consists of monitoring process parameters (e.g., process air flow, volume, humidity) [4]. The progress of drying is determined by the outlet air and granule bed temperature combined with the drying time. Fluid bed granulation endpoint is reached when a pre-set exhaust air temperature is obtained. However, also direct

product property measurements (e.g., moisture, particle size distribution, material solid state) should be considered.

Both spatial filter velocimetry (SFV) [5-14] and focused beam reflectance measurement (FBRM) [15-17] are able to record in real-time any changes to the particle size and its distribution during granulation. These sizing techniques provide a picture of granule growth and breakage as a function of granulation time by measurement of the particle chord lengths. A chord length is defined as the straight line between any 2 points on the edge of a particle. The measuring principle of SFV consists of an extended spatial filter method based on the shadows created onto a detector by the movement of particles through a laser beam [18, 19]. From these shadows, the particle chord length distribution and velocity are simultaneously extracted. FBRM uses the laser beam light backscattered into the probe when the beam crosses the surface of a particle [20, 21]. Multiplication of the duration of each reflection by the known velocity of the scanning beam results into a chord length measurement. Both techniques do not require any calibration. Whereas the FBRM C35 probe is equipped with a mechanical scraper on the sapphire measurement window to prevent probe fouling, the SFV probe utilizes a pressurized air connection to keep the measurement windows clean and disperse the particles.

The binder liquid addition and distribution affects the granule bed moisture level during granulation, contributing to the agglomeration process. The end product residual moisture content influences directly the granule properties, the subsequent post-granulation process steps (e.g., tabletting) and the product stability during storage. Near infrared (NIR) spectroscopy is highly suitable to evaluate moisture in-line during granulation [22]. The NIR spectral region is defined as the area across the wavenumber range 12500 – 4000 cm^{-1}. The molecular NIR light absorptions are mainly due to overtone and combination bands of fundamental vibrations in the MIR region [23]. As primarily vibrations of C-H, O-H, S-H and N-H bonds are observed, water exhibits strong absorption bands in an NIR spectrum. NIR measurements are non-destructive and the instrumentation exhibits a high

measurement speed and robustness. Besides chemical product information, NIR spectroscopy is also sensitive to physical (e.g., particle size) sample properties which are both quantitatively and qualitatively interpretable [24, 25]. Hence, NIR spectroscopy has been extensively used for in-line fluid bed granulation monitoring [8, 26-28], comprising (end product) moisture content [8, 24, 26, 27, 29-36] and/or granule size [24, 26, 29, 31].

This article describes the results of three case studies conducted consecutively, in order to develop a process control strategy for a top-spray fluid bed granulation process. Figure S1 (see Supplementary data) displays the experimental setups for the 3 case studies. Real-time granule size distribution information was provided via the implementation of an SFV probe directly into the process environment in case studies A and B, while in case study C an FBRM probe was (identically) installed in the granulator. Simultaneously, NIR spectra were collected at-line (case study A) and in-line (case studies B and C). The rapid data collection offered by these PAT tools enables real-time granulation analysis to control the manufacturing process.

The feed-forward process control strategy developed in this study uses the in-line collected granulation information during the spraying phase, to determine the optimum process setting (drying temperature) of the consecutive drying phase. Via real-time collection of process (i.e., spraying temperature and spray rate) and product (i.e., granule size distribution and moisture) parameters during the spraying period, the batch density is predicted early-on, i.e., at the end of the spraying cycle. When the predicted density does not meet the desired value, the control method proposes the use of an adjusted drying temperature leading to the desired granule density at the end of the granulation process. In all case studies, 2 steps were taken to develop this feed-forward control method:

(i) Using design of experiments (DoE), individual regression models for prediction of bulk and tapped density were developed based on 3 process parameters, *i.e., spraying temperature, spray rate and drying temperature*.

(ii) The development of a partial least squares (PLS) model to predict the end product density (**y**) from the granulation process and product information (**X**) collected during the spraying period. Separate PLS models were developed for bulk and tapped density.

The resulting control strategy combines the PLS density prediction model with the design regression equation, as is explained later in the manuscript.

Besides the development of a fluid bed granulation feed-forward control method, a quantitative PLS model for in-line moisture content prediction of the granulated end product was built using the NIR data.

2. Materials and methods

2.1. Materials

Each batch, consisting of dextrose monohydrate (700 g, Roquette Frères, Lestrem, France) and unmodified maize starch (277.5 g, Cargill Benelux, Sas van Gent, The Netherlands), was granulated with an aqueous binder solution of Tween 20 (2.5 g, Croda Chemicals Europe, Wilton) and hydroxypropylmethylcellulose (HPMC) (20 g, type 2910, Dow Chemical Company, Plaquemine-LA, USA). Two different HPMC viscosities were used, namely 15 mPa s (case studies A and C) and 5 mPa s (case study B). Each batch consisted of a total amount of solids of 1000 g. The HPMC binder was always sprayed as a 4% (w/w) solution.

2.2. Process description

Granulations were performed in a laboratory-scale fluid bed granulator (GPCG 1, Glatt, Binzen, Germany). A 1.2 mm diameter nozzle was installed top-spray at a height of 26 cm from the distributor plate. The binder liquid was atomized using a pressure of 1 bar during all granulations. Granulator filter bags were shaken every 45 s for a period of 7 s to prevent the entrapment of particles in the bags. The inlet air temperature during the spraying phase, the spray rate and the inlet air temperature during the drying phase were varied according to a 2-level full factorial design with three centre point repetitions (i.e., 11 granulation experiments, see Table 1). Inlet air, product

and exhaust air temperatures were manually recorded every minute during the entire granulation processes. The process was stopped when an outlet air temperature of 37°C and a product temperature of 45°C were obtained.

2.3. Collection of granule information during processing

2.3.1. Case study A: in-line SFV and at-line NIR spectroscopy

A spatial filter velocimetry probe (Parsum IPP 70, Gesellschaft für Partikel-, Strömungs- und Umweltmesstechnik, Chemnitz, Germany) was installed in the fluid bed granulator at a height of 20 cm and at approximately 5 cm from the sidewall of the granulator (Figure S1a, Supplementary data). Particles passed through an aperture with 4 mm diameter and an internal (20 L/min) and external (3 L/min) pressurized air connection were used to disperse the particles and prevent fouling of the measurement zone by the moist product. The experimental set-up was optimized in a previous study, enabling representative size measurements without disturbing the process [5]. Measured raw data were collected via an A/D converter. The software (In-line Particle Probe V7.12a) operated in the Windows XP environment. The SFV technique expresses the measured particle size distribution as a sieve distribution and via size percentiles (x01, x10, x25, x50, x63, x75, x90, x99). The sieve sizes are selected prior to executing the experiments and cannot be changed afterwards. During the entire granulation process, particle size measurements were continuously performed and an average particle size distribution was saved every 10 seconds.

At the end of each spraying cycle, a sample was withdrawn from the granulated mass via the built-in sample thief. The sample was at-line measured with diffuse reflectance NIR spectroscopy using a Nicolet Antaris II FT-NIR analyzer (Thermo Fisher Scientific, USA) equipped with an InGaAs detector and a quartz halogen lamp. The instrument was furnished with an integrating sphere module and controlled with the software package RESULT 3.0. The sampled granules were poured in the NIR instrument's sample cup, after which the sample cup was placed on the detection window of the integrating sphere. By rotating the cup in between NIR spectra collection, each sample was

measurement at 3 different positions. All spectra were collected in the 4000 – 10000 cm^{-1} spectral region with a resolution of 8 cm^{-1} and averaged over 32 scans. Background was measured using the gold-plated inner wall of the integrating sphere.

2.3.2. Case study B: in-line SFV and in-line NIR spectroscopy

The granule size distribution was collected in real-time by implementing the SFV probe in the fluid bed granulator identically to the setup described in 2.3.1. (case study A).

In-line diffuse reflectance NIR spectra were continuously collected during granulation by use of an FT-NIR spectrometer. The NIR instrument described in 2.3.1. was used and equipped with a fiber-optic non-contact probe for in-line measurements. Spectra were acquired every 20 seconds in the 4000 – 10000 cm^{-1} spectral region with a resolution of 8 cm^{-1} and averaged over 32 scans. Background was measured holding a golden plate (dimensions 7.6 cm x 2.5 cm) to the measurement window of the probe. The NIR probe was mounted into the granulator at a height of 7 cm (identical to the height of the system integrated sampling thief) and depth of 0.5 cm (Figure S1b, Supplementary data).

2.3.3. Case study C: in-line FBRM and in-line Lighthouse NIR spectroscopy

The granule size distribution was continuously monitored by implementing a focused beam reflectance measurement probe (model C35, Mettler Toledo, Columbus (Ohio), USA) in the fluid bed granulator (Figure S1c, Supplementary data). The pressurized air activated scraper cleaned the probe window every 2 s and the acquisition parameters were set to save the average particle size distribution every 10 s using a scan speed of 4 m/s. The FBRM probe was positioned at a height of 20 cm (identical to the SFV probe) and depth of 3 cm inside the fluid bed container. Due to the location of the FBRM measurement window at the probe tip, the instrument was inserted with a smaller depth compared to the SFV probe. Nevertheless, FBRM and SFV measurements were performed at identical locations since SFV windows are approximately 2 cm distant from the probe tip.

In-line diffuse reflectance NIR spectra were continuously collected during granulation using an FT-NIR spectrometer (MATRIX^{TM}-F Duplex, Bruker Optics Ltd., UK) equipped with a fiber-optic Lighthouse Probe^{TM} (LHP, GEA Pharma Systems nv – Collette, Wommelgem, Belgium). The LHP is an immersion probe with seven radial windows that radiate and collect light. Hence, sampling is performed 360° around the probe. The spectrometer operated in the 4000 – 10000 cm^{-1} NIR region and spectra with a resolution of 8 cm^{-1} and averaged over 32 scans were continuously collected. The NIR measurements in case studies B and C were performed at identical locations inside the granulator, but the NIR LHP had to be inserted with a greater depth as the measurement windows are positioned 3.75 cm from the probe tip (the measurement window of the NIR probe used in case study B was located at the probe tip itself). The close proximity of the NIR probe to the bottom of the fluid bed granulator ensured a measurement position with continuous dynamically flowing material in front of the probe window. However, this also introduced the danger of modifying the airflow pattern in the granulator and consequently the agglomeration process. Figure S2 (see Supplementary data) displays the off-line sieve analysis results of batches 2, 1 and 7 granulated in case studies A and C to show the effect of implementing the NIR LHP. Batch 2 was granulated using a spraying temperature of 50°C and spray rate of 12 g/min (Table 1). The perfect agreement between batch 2 sieve distributions for case studies A and C proved that the NIR LHP did not influence the agglomeration process under low-moisture spraying phase conditions. However, the particle size distributions of batch 1 and particularly batch 7 (granulated at an inlet air temperature of 30°C and spray rate of 12 respectively 20 g/min) shifted to larger sizes in case study C. Hence, the influence of the NIR LHP on the granulation process was more pronounced using medium- and high-moisture granulation conditions. The probe significantly disturbed the airflow pattern and consequently the simultaneous process of heat and moisture transfer during granulations with a low spraying temperature and/or a fast spray rate. Therefore, the granulation liquid was not efficiently evaporated and overwetted granules were produced.

Although the information provided by the in-line FBRM and NIR LHP in case study C described the different stages of granulation and allowed to monitor the process, the design and/or location of the NIR LHP was not suitable for the laboratory-scale fluid bed granulator. Hence, it was impossible to generate a feed-forward control strategy for case study C.

2.4. Characterization of granules

2.4.1. Karl Fischer titration

Reference moisture content of the granule batches was determined off-line using a V30 volumetric Karl Fischer titrator (Mettler Toledo, Gießen, Germany). Hydranal®-Composite 5 (1-component, Sigma-Aldrich, Germany) was used as titrant and Hydranal®-Methanol dry (Sigma-Aldrich, Germany) as solvent. Three Karl Fischer determinations were performed for each completed batch. The water content in samples was determined via the quantitative reaction of water molecules with iodine and sulfur dioxide in the presence of methanol and imidazole as base. The amount of iodine consumption as a result of the reaction with water was measured.

2.4.2. Density measurements

The bulk density and tapped density were determined for each completed batch. Twenty-five g samples were gently poured into a 100 mL graduated cylinder. By use of the granule weight and volume, bulk density was calculated. Next, each sample was tapped 1250 times employing an automatic tapper (J. Engelsmann AG, Ludwigshafen am Rhein, Germany) and the new volume was used to determine the tapped density. All density measurements were performed in triplicate and the average density was calculated.

2.5. Development of the granulation feed-forward control strategy

In-process measurements of the agglomerates' properties, performed during the spraying phase of the batch process, were used to predict end product granule characteristics (bulk and tapped density) using a PLS model (see *(ii)* below). When these predicted densities were not as desired, the drying temperature of the successive drying phase was adjusted. The extent to which the drying

temperature had to be adjusted was derived from a DoE model (see *(i)* below), expressing the granule bulk and tapped density as function of the spraying temperature, spray rate and drying temperature.

(i) A 2-level full factorial design (see 2.2. and Table 1) was carried out, resulting in a polynomial regression model (considering the 3-factor interaction term negligible) for each response:

$$y = \beta_0 + \beta_1 x_1 + \beta_2 x_2 + \beta_3 x_3 + \beta_{12} x_1 x_2 + \beta_{13} x_1 x_3 + \beta_{23} x_2 x_3 \qquad (1)$$

with y the response *(i.e., bulk or tapped density)*, $x_{1\text{-}3}$ the coded process variables *(the inlet air temperature during the spraying phase, the spray rate and the inlet air temperature during the drying phase)*, β_0 the intercept and β_i the model coefficients expressing for each factor how much the response is affected by changing the factor from the coded DoE level 0 to +1. Individual regression models were developed for bulk and tapped density. The authors acknowledge that the use of a central composite design might improve the predictive capability of the models, as each factor is then varied on five experimental levels instead of three. Analysis of the design experiments and development of the DoE models were done with the MODDE software (Version 9.0, Umetrics, Umeå, Sweden).

(ii) Partial least squares models were built using the SIMCA-P+ software (Version 12.0.1, Umetrics, Umeå, Sweden), correlating two data matrices, **X** and **y**. The **X**-matrix contained granulation information collected during the spraying period of the 11 DoE batches, while the **y**-vectors consisted of the design responses, bulk and tapped density. Individual PLS models were developed for bulk and tapped density. Applying these PLS models during new granulations allows predicting the density of a completed batch (i.e., after spraying and drying phase) at the end of the spraying period.

Hartung et al. [8] reported that not only residual moisture in granules affected subsequent process steps, but also the moisture profile of the entire granulation process. Hence a similar approach, examining whether the complete spraying phase fingerprint contributed to the

predictability of the density models, was considered. Therefore, the 3-way data matrix of [*design batches (I)] x [collected granulation process and product variables (J)] x [spraying time (K)]* was unfolded in the direction of the batches, creating a 2-way data matrix [*design batches (I)] x [collected granulation process and product variables x spraying time (J x K)]* (Figure S3, see Supplementary data) [37]. In that way, the **X**-matrices of the developed PLS models contained 11 rows, corresponding to the 11 design batches, and the number of columns depended on the included spraying phase time-period. This resulted in the development of several PLS models (for bulk and tapped density individually), differing in the number of **X**-matrix columns describing the collected spraying phase data:

- Case study A – In-line SFV and at-line NIR measurements: The first 3 **X**-matrix columns for the various PLS models developed in case study A contained the settings of the 3 process variables (spraying temperature, spray rate and drying temperature) describing the collected granulation *process* data. The following columns of models M0 and M1 consisted of the collected granulation *product* information (based on SFV and NIR measurements) at the end of the spraying phase (i.e., when all granulation liquid has been sprayed) (Figure 1a). Hence, the **X**-matrix of model M0 contained the 3 process variables and the in-line SFV measured granule size. The 8 percentile descriptors (see 2.3.1) were used to express the granule size distribution as the size of the smallest SFV sieve was set to 200 µm, which was too large to capture the size distribution variations between the different experiments.

  The **X**-matrix of model M1 was identical to the M0 **X**-matrix, complemented with the at-line collected NIR information. To express the NIR captured spectral variation between the 11 design batches, principal component analysis (PCA) was performed on all at-line collected NIR spectra *(3 spectra x 11 batches)*. The score values on the principal components (PC1 and PC2) were added to the M1 **X**-matrix.

  Models M2-M9 were built by adding each time the granule size distribution collected during the previous spraying phase minutes to the **X**-matrix (Figure 1a).

- Case study B – In-line SFV and in-line NIR measurements: The M1 **X**-matrix included the 3 process variables, the granule size distribution and the NIR data (expressed by PCA scores) collected at the end of the spraying phase, as described above for case study A. Based on the granule sizes measured in case study A, the SFV sieves were correctly selected and used to describe the collected granule size distribution during granulation (Figure 1b).

  Since both SFV and NIR measurements were continuously performed, M2-M5 **X**-matrices contained both types of granule product information collected during the previous spraying phase minutes (Figure 1b).

The goodness of fit and the predictive power of the PLS models were given by R^2 and Q^2. R^2 expresses the percent variation of the response explained by the model and Q^2 measures how well the model is able to predict the examined response for new experiments (test batches). In addition to the evaluation of R^2 and Q^2, the root mean square errors of estimation (RMSEE) and root mean square errors of prediction (RMSEP) were compared to select the best PLS prediction model. Both errors indicate the difference between the experimentally measured value and the value predicted by the model under examination, for the calibration and test batches respectively.

The feed-forward control strategy, guaranteeing the granule quality of future experiments, combines the optimal predictive PLS model with the DoE regression equation. When a new granulation process is started, the selected PLS model allows the prediction of the end product quality (i.e. density of the end product) at the end of the spraying period based on the real-time collected granule information. If the predicted density does not meet the predefined quality requirements, the DoE model terms (Eq. 1) expressing the influence of the drying temperature on the batch density (i.e., $\beta_3 x_3$, $\beta_{13} x_1 x_3$, $\beta_{23} x_2 x_3$) can be used to calculate by how many (coded) units the drying temperature should be adjusted to lead the granulation process towards the desired density. To exemplify, if the predicted density differs from the desired density by *A* g/mL, then the level of the pre-set nominal drying temperature (x_3, coded according to the performed DoE) should be adjusted

with Δ units (coded as above) established by the following equations (expressed with coded DoE variables and corresponding coefficients):

$$y + A = \beta_0 + \beta_1 x_1 + \beta_2 x_2 + \beta_3 (x_3 + \Delta) + \beta_{12} x_1 x_2 + \beta_{13} x_1 (x_3 + \Delta) + \beta_{23} x_2 (x_3 + \Delta) \quad (2)$$

$$A = \beta_3 \Delta + \beta_{13} x_1 \Delta + \beta_{23} x_2 \Delta \quad (3)$$

$$\Delta = \frac{A}{\beta_3 + \beta_{13} x_1 + \beta_{23} x_2} \quad (4)$$

2.6. Development of an NIR method to predict end product moisture content

A quantitative NIR calibration model for in-line moisture content prediction of the granulated end product in case study B was developed. Calibration and validation batches were manufactured by granulation of the previously described formulation (2.1.), and terminating the drying period at different exhaust air temperatures to create granules with varying moisture levels. Subsequently, the fluid bed container was removed from underneath the filter housing and by immersion of the NIR probe in the granule bed, static NIR spectra were at-line recorded (at different locations in the bed). The moisture reference value was determined by Karl Fischer titration using the average of three measured samples. In total, 20 NIR spectra of each batch were correlated with the Karl Fischer determined moisture content using PLS regression. The calibration model covered a water content range between 4% and 10% including 9 concentration levels. In the diffuse reflectance measurement, the light travels various distances because the distribution of sample particles and particle sizes are different. Hence, prior to modeling the absorbances in the 4500 – 7500 cm^{-1} spectral region of 180 NIR spectra, standard normal variation (SNV) correction was performed to eliminate these scattering effects and the spectra were mean centered. The calibration of the PLS model was evaluated by calculation of the RMSEE. The model was externally and independently validated by computing the RMSEP using 140 spectra of 7 validation batches.

3. Results and discussion

3.1. Case Study A: in-line SFV and at-line NIR spectroscopy

For the 11 DoE granulations performed in case study A, batch bulk and tapped densities were determined in triplicate and averages were used as design responses. Individual bulk and tapped density multiple linear regression models were computed and the significance of the coefficients was determined by calculation of the 95% confidence interval. The confidence intervals of the three 2-factor interaction coefficients included zero indicating the statistical insignificance of the interactions. The insignificant coefficients were removed and the following bulk density (BD) and tapped density (TD) regression equations (based on the coded variables) were obtained after refitting the models:

$$BD = 0.4357 - 0.0268 * T_{spraying} + 0.0204 * spray\ rate - 0.0196 * T_{drying} \quad (5)$$

$$TD = 0.5307 - 0.0258 * T_{spraying} + 0.0181 * spray\ rate - 0.0284 * T_{drying} \quad (6)$$

As described in 2.5., separate PLS models were developed for bulk and tapped densities (**y**) to predict the densities of a completed batch (i.e. after spraying and drying phase) based on the collected data during the spraying period (Figure 1a). Therefore, all available granulation *process* and *product information* related to batch density were included in the PLS **X**-matrices. Herewith, the settings for the 3 process variables (i.e., spraying temperature, spray rate and drying temperature) were included as they significantly influenced end product density according to the DoE analysis. Furthermore, since the density of a product is defined as the mass of the material divided by the volume the material occupies (i.e., volume of individual particles, inter-particle volume and the internal pore volume), the granule size distribution during the spraying phase is related to batch density. Consequently, the **X**-matrix of the initially constructed PLS model (model M0, Figure 1a) included the 3 process variable settings and the particle size distribution determined at the end of the spraying period.

Principal component analysis was performed on all NIR spectra collected for the 11 design batches to examine the spectral differences between the batches. Using the SNV corrected 4500 – 7500 cm^{-1}

spectral region, a model consisting of 2 principal components (PC1 and PC2), describing 99.9% of the spectral variation was computed. The PC1 and PC2 loading plots exhibited large contributions by the 7000 cm^{-1} and 5200 cm^{-1} spectral regions, corresponding to the NIR absorption bands of water. The PC1 versus PC2 scores plot showed clustering of the design experiments along PC1 describing the variability in granule moisture level caused by the process settings of the granulation cycles (Figure 2). Experiments performed at a low spraying temperature and a high spray rate (-1,1; high granule moisture) clustered in the outer positive region of PC1, while experiments executed using a high spraying temperature and low spray rate (1,-1; low granule moisture) grouped in the negative part of PC1. Combinations of spraying temperature and spray rate resulting in a moderate granule moisture state (1,1 ; 0,0 ; -1,-1) lay around the PC1 origin. Hence, instead of including all NIR spectral variables, only the PC1 and PC2 scores were added to the PLS **X**-matrix (model M1, Figure 1a) comprising the NIR captured granule moisture differences between the various batches. The addition of the granule size distributions collected during the preceding spraying phase minutes resulted in the development of models M2, M3, ..., M9 (Figure 1a).

Figure 3 displays the resulting R^2, Q^2, RMSEE and RMSEP values for the developed BD and TD PLS models M0 to M9. The calculation of the prediction error (RMSEP) was based on the predicted densities of 4 new independent batches (not included in the calibration set). Four randomly selected batches from the performed DoE, namely batch 4, 8 and twice the centre point, were granulated a second time covering drying temperatures of 50°C, 70°C and 60°C. The bulk and tapped density R^2 and Q^2 values lay in the same range, with repeatedly higher values for BD models. Adding PCA scores distinctively increased the models' predictability based on about 10% rise in Q^2 values between M0 and M1. Adding the granule size distributions collected during the complete spraying phase to the X-matrices improved only slightly the predictability. Maximum Q^2 was reached by models M3 and M4. According to the estimation and prediction errors, optimal density prediction resulted from the granule information collected at the end of the spraying period. Adding the full particle size fingerprint collected during spraying did not seem to contribute to a better predictability.

The feed-forward control strategy described in 2.5. requires (i) a *valid prediction of the batch density* after completion of the spraying period, and (ii) a *reliable estimation of the optimal drying temperature* to obtain the desired density, using the DoE regression equation. The latter was assessed for the previously mentioned 4 test batches by means of Eq. 1. Hence, the drying temperature (x_3) was computed applying the predicted BD (y), the significant regression coefficients (β_i) and the experimentally set spraying temperature (x_1) and spray rate (x_2). The BD values predicted by all 9 PLS models (M0 to M9) were used in these calculations and identical computations were carried out based on the predicted TDs. As the drying phase of the 4 test batches was experimentally executed, these calculated drying temperatures were compared to the drying temperatures applied during processing (Table 2). The drying temperature predictions were satisfactory, keeping in mind that an increase in drying temperature by 1°C, reduces the BD and TD by 0.0020 g/mL and 0.0028 g/mL respectively. In general, the accuracy of drying temperature prediction tends to decrease going from M0 to M9, caused by the growing incorrectness in batch bulk and tapped density predictions when adding spraying phase information collected early in the process (Figure 3).

3.2. Case Study B: in-line SFV and in-line NIR spectroscopy

3.2.1. Qualitative monitoring of the granulation process

In-line SFV measurements were appended with in-line NIR spectra collection during the 11 design granulations to describe the continuously evolving granule size and moisture. Figure 4a-d exemplifies the change in NIR spectra and SFV measured average particle size (D50) during one of the performed DoE experiments (batch 3).

Examination of the raw NIR data without preprocessing (Figure 4a) showed that spraying of the binder liquid onto the fluidizing bed, caused a significant increase in spectrum baseline, most likely due to the increasing particle size [30, 38]. During subsequent drying, water removal and attrition decreased the granule size and therefore influenced the physical state of the measured samples. This was associated with a lowering of the NIR spectrum baseline.

By SNV preprocessing of the NIR spectra, physical light-scattering effects were removed from the chemical light absorbance effects in the spectra [39, 40]. Figure 4b and 4c display the NIR spectra collected during the spraying and drying operation, respectively, after SNV preprocessing. The color assignment to the spectra is related to the spraying and drying times with dark and light coloring indicating the start, respectively the end of the cycle. The spectral evolution was characterized by a strong increase and subsequent decrease in NIR absorptions in the 5200 cm^{-1} and 7000 cm^{-1} spectral region. These regions are associated with the OH combination band of the fundamental stretching and deformation vibration, and the first overtone of the OH bond in water, respectively. The signal in the first overtone region for CH, CH_2 and CH_3 around 5700 – 6000 cm^{-1} decreased during spraying and increased throughout drying.

The PC1 obtained after principal component analysis on the SNV corrected spectra (4500 – 7500 cm^{-1} spectral region) accounted for 90% of the spectral variation. Similarity between the PC1 loading profile and the NIR spectrum of water confirmed the association of this component with the water addition/removal during the granulation process. The trajectory of PC1 scores as a function of granulation time (Figure 4d) displayed a clear distinction between the 3 granulation process steps. During heating and powder mixing (step I, data shown of the final minute), the score values were similar. The addition of binder liquid in the second step increased the PC1 scores, while drying of the granules caused a score value decrease until a minimum value was reached similar to the PC1 scores in step I. The trajectory of SFV collected D50 values during granulation exhibited a similar sequence of the three granulation process steps. A constant particle size during sample agitation and heating was followed by a particle size increase during the spraying of binder liquid. Drying slightly reduced the average granule size due to inter-particle and particle-fluid bed container collisions. As can be seen from Figure 4d, the variation in NIR scores and SFV measured particle size during granulation provided improved knowledge on the batch evolution. A better insight into the granulation under examination is achieved, compared to the traditionally used product and exhaust air temperature control charts. Figure 4e shows that after approximately 8 minutes in the spraying period, the

process variables did no longer provide information on the granulation progress as product and exhaust air temperatures remained constant. During routine production, the use of a plot expressing particle size and moisture content trajectories (Figure 4d) allows determining whether a batch is developing under the normal operating conditions and granulation is being performed accordingly [6].

3.2.2. Development of the granulation feed-forward control strategy

After executing the 11 design granulations, end product bulk and tapped density were determined and the coefficients of the significant main and interaction effects calculated. The following bulk density and tapped density regression equations (based on the coded variables) were obtained:

$$BD = 0.4733 - 0.0332 * T_{spraying} + 0.0236 * spray\ rate - 0.0164 * T_{drying} + 0.0107 * T_{spraying} * spray\ rate \quad (7)$$

$$TD = 0.5744 - 0.0211 * T_{spraying} + 0.0096 * spray\ rate - 0.0246 * T_{drying} + 0.0207 * T_{spraying} * spray\ rate \quad (8)$$

To construct bulk and tapped density PLS models, a similar methodology as for case study A (3.1.) was followed, however with one difference. In addition to the granule size, NIR spectra were continuously in-line collected during the entire DoE granulation processes. Principal component analysis was performed on the SNV corrected 4500 – 10000 cm^{-1} spectral region of all collected NIR spectra (for all batches) to examine the NIR captured granule differences between the 11 design batches. The NIR variables contributing most to the 2 first principal components were associated with the two water bands. Hence the scores on PC1 and PC2 were added to the PLS **X**-matrices to describe the granule moisture information captured by in-line NIR spectroscopy. Figure S4 (see Supplementary data) displays the RMSEE and RMSEP values of the resulting bulk density PLS models M1 to M5, without and with the inclusion of NIR scores in the **X**-matrix. Since case study A showed that the information collected during the final minutes of the spraying period produced the best BD predictions, only 5 PLS models were developed using the granule size and moisture information

collected at the end of spraying, augmented with the granule data collected during the final 4 minutes of spraying (i.e., models M1 to M5). To calculate the prediction error, 4 new batches (i.e., batch 1, 5 (twice) and 8), not included in the calibration set were granulated a second time. The resulting RMSEE values decreased by the addition of NIR information, while RMSEP values exhibited a more random trend.

As a result, taking Figure S4 (see Supplementary data) into account, the **X**-matrices of the developed BD and TD PLS models in case study B were composed of continuously collected granule size and moisture data (Figure 1b). The resulting BD and TD PLS models showed excellent fit and predictability, with the BD models producing slightly higher R^2 and Q^2 values (Figure 5). Both BD and TD models showed that the addition of size and NIR information collected during the final minutes of the spraying period, improved the fit and predictability of the calibration batches as R^2, Q^2 and RMSEE values reached a maximum respectively minimum for model M5. The density prediction of new, independent batches did not exhibit an identical trend. The initial addition of granule information resulted into a small decrease in prediction error. Further inclusion of **X**-variables did not benefit the predictions and tends to indicate overfitting. For both BD and TD, the models fit the data well, but TD predictions are less good, indicating an improved correlation between the collected granule information and the free bulk density. These results are consistent with the observations made in case study A.

Next to the valid prediction of batch density from the data collected during the spraying phase, the reliable estimation of the optimal drying temperature resulting in the required density was assessed. This was initially examined by calculating the drying temperatures using the PLS predicted BD and TD values of the 4 test batches (for the 5 PLS models), in combination with equations 5 and 6 respectively. The drying phases of the 4 batches were experimentally completed, which allowed the comparison between the predicted and the applied drying temperature (Table 3). The correctness in temperature prediction based on predicted BD was comparable to the results in case study A. The

computed drying temperatures based on predicted TD however displayed a larger bias, probably due to the notable higher TD prediction error (Figure 5).

In case studies A and B, the ability of the developed PLS models to predict the density of future batches was evaluated using test batches not included in the calibration set. Hence, a primary selection of the **X**-variables correlating with the batch density was made. Comparing the predicted drying temperature (from implementing the PLS predicted density in the DoE models) with the experimentally applied temperature allowed a first assessment of the suitability of the proposed feed-forward strategy. In a next step, the developed methodology was tested during the granulation of new batches. To predict the batch quality at the end of the spraying period and adjust/correct the granulation progress during drying, BD PLS models were combined with the BD DoE regression equation similar to case study A.

Batch CS *(control strategy)* was granulated using an inlet air temperature of 30°C and binder addition rate of 12 g/min during the spraying period. The subsequent drying phase was executed at an inlet air temperature of 50°C. Throughout the complete granulation process, granule size data and NIR spectra were continuously collected. The acquired granulation information was used to predict the batch bulk density using models M1 to M5. Hence, by use of the 2 spraying period parameters, the in-line collected product information and the intended use of an inlet air temperature of 50°C during drying, the bulk density of the completed batch was predicted at the end of the spraying period. Drying of batch CS at an inlet air temperature of 50°C enabled the comparison between this early-on predicted BD and the experimentally measured value (Table 4, batch ID CS). The excellent agreement between the measured BD (after batch production) and the predicted BD (at the end of the spraying period) for models M1 to M3 demonstrated the validity of the developed PLS models. The predicted BD values by models M4 and M5 are also in close agreement with the measured BDs, but exhibit a slightly larger deviation compared to M1 – M3 predictions.

Next, the use of the developed BD DoE regression equation to determine the optimal drying temperature was examined. We decided that granulation of batch CS should give a BD of 0.48 g/mL

instead of 0.52 g/mL. The adjusted drying temperature resulting in a BD decrease of 0.04 g/mL, was calculated by use of equation 4. Keeping in mind that the values of the process variables and coefficients are expressed according to the DoE scaling (i.e., spraying temperature of *-1* and spray rate of *-1*), the following calculations were performed:

$$adjusted\ x_3 = x_3 + \Delta = x_3 + \left[\frac{-0.04}{\beta_3 + \beta_{13}x_1 + \beta_{23}x_2}\right]$$

$$adjusted\ x_3 = -1 + \left[\frac{-0.04}{-0.0164 + (-0.00258 * -1) + (0.009275 * -1)}\right] = 0.7$$

The experimental drying temperature levels of 50°C, 60°C and 70°C were coded to -1, 0 and 1 according to the DoE (Table 1). Hence, conversion of the coded into the uncoded value, shows that the pre-set drying temperature of 50°C should be increased to 67°C to obtain the desired BD:

$$0.7\ (coded) = 60\ °C + (10 * 0.7) = 67\ °C\ (uncoded)$$

Therefore, batch CS was granulated twice more using identical spraying phase settings and a drying temperature of 67°C (i.e., batch CS adjusted a and b). Table 4 displays the predicted bulk density based on the process settings (drying temperature of 50°C) and the collected granule information at the end of the spraying period. According to the predictions by M1 – M3, this would result for both batches into a BD of 0.52 g/mL as observed for batch CS. However, as we aimed to obtain a BD of 0.48 g/mL, a temperature of 67°C derived from the BD DoE regression equation was applied during drying. The subsequent experimental BD value measurements of 0.48 g/mL was consistent with the desired density.

These results suggest that the developed BD PLS model allowed a reliable prediction of batch density using granule information collected during the end of the spraying period (M1 – M3). The granule behavior fingerprint during the complete granulation cycle did not improve the predictions. By use of the BD design equation, the granulation process could be adjusted during drying (adjusted drying temperature), hence guiding the process towards the desired density.

3.2.3. Development of an NIR method to predict end product moisture content

The developed PLS calibration model for end product moisture content prediction (described in 2.6.1.) exhibited an RMSEE and RMSEP of 0.51% and 0.47% respectively. Optimum moisture content predictions were obtained using 2 PLS factors. In the selected predictive model, 94% of the spectral variance was correlated with 87% of the water variation. The calibration model was applied to the in-line collected NIR spectra of the 11 design batches. The moisture content predicted during the final minute of drying was compared to the reference moisture content determined by Karl Fischer titration (Table 5). The in-line predictions were attended with an RMSEP of 0.51%, comparable to the error of the calibration model. Hence, although the calibration model was developed by use of statically recorded NIR spectra, the model was also applicable to dynamically collected spectra.

In addition to the in-line collected NIR spectra, 20 at-line NIR spectra were recorded per design batch after granulation. At-line moisture content predictions resulted in an RMSEP of 0.43%. Similar in-line and at-line prediction errors suggest that the continuous flow of particles during in-line NIR spectra collection did not reduce the predictability of the NIR measurements. It also implies that the moisture predictions were not affected by the build-up of material on the probe using these granulation process conditions. Since no cleaning device was used, the NIR window was probably continuously cleaned by the product itself during fluidization.

4. Conclusions

This work aimed to develop a fluid bed granulation control strategy based on real-time collected process and product information. The developed feed-forward control strategy uses granulation information collected during the spraying phase to determine the optimal drying phase temperature, hence ensuring end product density.

The finalized control strategy *(case study B)* applied an in-line SFV and NIR probe to continuously collect granule size and moisture data. The developed BD PLS model enabled a good prediction of batch BD by use of the granule size distribution and NIR data collected at the end of the spraying

period. Addition of granule product information collected during the complete granulation cycle did not improve the predictions. Applying the BD DoE regression equation information, the granulation process was modified during the drying period to meet the quality requirements. In addition, the SFV measurements and NIR data allowed the clear distinction between the three different stages of a granulation process. Through the development of a quantitative NIR moisture calibration model, adequate in-line prediction of batch end product moisture levels was achieved.

Hence, the results showed that by combining particle size (SFV) and moisture (NIR) trajectories, real-time monitoring of the granulation progress was accomplished. The real-time measurement of end product particle size and prediction of its moisture content enabled in-line granule quality analysis. In addition, the adjustment of granulation progress during drying to meet the desired bulk density requirements showed that full control of the granulation process is possible by use of SFV and NIR spectroscopy. Implementation of the (automated) control strategy should result into the production of high quality batches at lower overall costs.

Acknowledgement

This work was financially supported by the Institute for the Promotion of Innovation through Science and Technology in Flanders (IWT-Vlaanderen).

References

[1] D.E. Wurster, J. Am. Pharm. Assoc. 48 (1959) 451.

[2] D.E. Wurster, J. Am. Pharm. Assoc. 49 (1960) 82.

[3] American Food and Drug Administration (FDA), Guidance for Industry PAT - A Framework for Innovative Pharmaceutical Manufacturing and Quality Assurance, FDA, 2004.

[4] D.M. Parikh, J.A. Bonck, M. Mogavero, in: D.M. Parikh (Ed.), Handbook of Pharmaceutical Granulation Technology, Marcel Dekker, Inc., New York, 1997, p. 227.

[5] A. Burggraeve, T. Van Den Kerkhof, M. Hellings, J.P. Remon, C. Vervaet, T. De Beer, Eur. J. Pharm. Biopharm. 76 (2010) 138.

[6] A. Burggraeve, T. Van den Kerkhof, M. Hellings, J.P. Remon, C. Vervaet, T. De Beer, Eur. J. Pharm. Sci. 42 (2011) 584.

[7] C. Fischer, M. Peglow, E. Tsotsas, Chem. Eng. Sci. 66 (2011) 2842.

[8] A. Hartung, M. Knoell, U. Schmidt, P. Langguth, Drug Dev. Ind. Pharm. 37 (2011) 274.

[9] J. Huang, C. Goolcharran, J. Utz, P. Hernandez-Abad, K. Ghosh, A. Nagi, J. Pharm. Innov. 5 (2010) 58.

[10] T. Närvänen, 19th Helsinki Drug Research, Helsinki, FINLAND, 2008, p. S12.

[11] T. Närvänen, T. Lipsanen, O. Antikainen, H. Räikkönen, J. Heinämäki, J. Yliruusi, J. Pharm. Sci. 98 (2009) 1110.

[12] T. Närvänen, T. Lipsanen, O. Antikainen, H. Räikkönen, J. Yliruusi, Int. J. Pharm. 357 (2008) 132.

[13] D. Petrak, S. Dietrich, G. Eckardt, M. Koehler, Adv. Powder Technol. 22 (2011) 203.

[14] S. Schmidt-Lehr, H.U. Moritz, K.C. Jurgens, Pharm. Ind. 69 (2007) 478.

[15] X.H. Hu, J.C. Cunningham, D. Winstead, Int. J. Pharm. 347 (2008) 54.

[16] J. Huang, G. Kaul, J. Utz, P.W. Hernandez, V., D. Bradley, A. Nagi, D. O'Grady, J. Pharm. Sci. 99 (2010) 3205.

[17] A. Tok, X.P. Goh, W. Ng, R. Tan, AAPS PharmSciTech, 9 (2008) 1083.

[18] D. Petrak, Part. Part. Syst. Char. 19 (2002) 391.

[19] D. Petrak, H. Rauh, Part. Sci. Technol. 24 (2006) 381.

[20] N. Kail, W. Marquardt, H. Briesen, Ind. Eng. Chem. Res. 48 (2009) 2936.

[21] A. Ruf, J. Worlitschek, M. Mazzotti, Part. Part. Syst. Char. 17 (2000) 167.

[22] M. Blanco, J. Coello, H. Iturriaga, S. Maspoch, C. de la Pezuela, Analyst, 123 (1998) 135R.

[23] Y. Roggo, P. Chalus, L. Maurer, C. Lema-Martinez, A. Edmond, N. Jent, J. Pharm. Biomed. Anal. 44 (2007) 683.

[24] F.J.S. Nieuwmeyer, M. Damen, A. Gerich, F. Rusmini, K.M. van der Voort, H. Vromans, Pharm. Res. 24 (2007) 1854.

[25] T. De Beer, A. Burggraeve, M. Fonteyne, L. Saerens, J.P. Remon, C. Vervaet, Int. J. Pharm. 417 (2011) 32.

[26] M. Alcala, M. Blanco, M. Bautista, J.M. Gonzalez, J. Pharm. Sci. 99 (2010) 336.

[27] R.L. Green, G. Thurau, N.C. Pixley, A. Mateos, R.A. Reed, J.P. Higgins, Anal. Chem. 77 (2005) 4515.

[28] J.T.T. Leskinen, M.A.H. Okkonen, M.M. Toiviainen, S. Poutiainen, M. Tenhunen, P. Teppola, R. Lappalainen, J. Ketolainen, K. Jarvinen, Chem. Eng. J. 164 (2010) 268.

[29] W.P. Findlay, G.R. Peck, K.R. Morris, J. Pharm. Sci. 94 (2005) 604.

[30] P. Frake, D. Greenhalgh, S.M. Grierson, J.M. Hempenstall, D.R. Rudd, Int. J. Pharm. 151 (1997) 75.

[31] S.G. Goebel, K.J. Steffens, Pharm. Ind. 60 (1998) 889.

[32] A. Peinado, J. Hammond, A. Scott, J. Pharm. Biomed. Anal. 54 (2011) 13.

[33] J. Rantanen, O. Antikainen, J.P. Mannermaa, J. Yliruusi, Pharm. Dev. Technol. 5 (2000) 209.

[34] J. Rantanen, S. Lehtola, P. Ramet, J.P. Mannermaa, J. Yliruusi, Powder Technol. 99 (1998) 163.

[35] J. Rantanen, E. Rasanen, O. Antikainen, J.P. Mannermaa, J. Yliruusi, Chemometr. Intell. Lab. Syst. 56 (2001) 51.

[36] J. Rantanen, E. Rasanen, J. Tenhunen, M. Kansakoski, J.P. Mannermaa, J. Yliruusi, Eur. J. Pharm. Biopharm. 50 (2000) 271.

[37] T. Kourti, J. Chemometr. 17 (2003) 93.

[38] J. Rantanen, J. Yliruusi, Pharm. Pharmacol. Commun. 4 (1998) 73.

[39] R.J. Barnes, M.S. Dhanoa, S.J. Lister, Appl. Spectrosc. 43 (1989) 772.

[40] I.S. Helland, T. Naes, T. Isaksson, Chemometr. Intell. Lab. Syst. 29 (1995) 233.

Table legends

Table 1. Overview of the performed design experiments (2-level full factorial design with 3 replicates of center point).

Table 2. Comparison of the experimentally applied drying temperature with the estimated optimum drying temperature for 4 test batches (case study A) using the process control methodology.

Table 3. Comparison of the experimentally applied drying temperature with the estimated optimum drying temperature for 4 test batches (case study B) using the process control methodology.

Table 4. Use of the developed granulation feed-forward control strategy. Comparison of the predicted bulk density (BD) at the end of the spraying period using a drying temperature of 50°C, with the experimentally measured bulk density applying a drying temperature of 50°C (batch CS) and 67°C (batch CS adjusted a and b).

Table 5. Moisture content (MC) and standard deviation determined using Karl Fischer (KF) and predicted by the near infrared PLS calibration model for the design granulations performed in case study B.

Figure legends

Figure 1. The **X**-matrix and **y**-vector for the developed bulk density and tapped density PLS models in case studies A (a) and B (b) (PSD = particle size distribution).

Figure 2. PC1 (R^2X = 98.4%) versus PC2 (R^2X = 1.5%) scores plot of the at-line collected NIR spectra for the 11 design experiments performed in case study A. The scores are labeled according to the coded DoE experiment settings for the spraying temperature and spray rate. Three NIR spectra were collected per design experiment.

Figure 3. R^2, Q^2, RMSEE and RMSEP for bulk density (BD) and tapped density (TD) PLS models M0 to M9 (case study A).

Figure 4. Granulation product and process information in-line collected during granulation of batch 3 (case study B). Pure NIR spectra collected during the mixing, spraying and drying steps of the granulation process (a). SNV corrected NIR spectra collected during the spraying phase (b) and drying phase (c). The color assignment to the spectra is related to the spraying and drying times with dark and light colors indicating the start, respectively the end of the cycle. Evolution of D50 and PC1 scores (d), and product and exhaust air temperatures (e) during the granulation process.

Figure 5. R^2, Q^2, RMSEE and RMSEP for bulk density (BD) and tapped density (TD) PLS models M1 to M5 (case study B).

Supplementary data

Figure S1. Front view schematic of the experimental setup in case studies A (a), B (b) and C (c). Standard components of the fluid bed equipment are indicated by numbers: filter bags (1), spray arm (2), spray nozzle (3), front window (4), sample thief (5).

Figure S2. Sieve distributions of batches 2, 1 and 7 granulated in case study A (solid line) and case study C (dashed line).

Figure S3. Unfolding of the 3-way granulation batch data matrix preserving batch direction.

Figure S4. RMSEE and RMSEP values of bulk density PLS models M1 to M5 with **X**-matrices containing the granule size distribution either without (wo) or with (w) the inclusion of NIR scores (case study B).

Table 1. Overview of the performed design experiments (2-level full factorial design with 3 replicates of center point).

Batch	Inlet air T during spraying (°C)	Spray rate (g/min)	Inlet air T during drying (°C)
1	30	12	50
2	50	12	50
3	30	20	50
4	50	20	50
5	30	12	70
6	50	12	70
7	30	20	70
8	50	20	70
9	40	16	60
10	40	16	60
11	40	16	60

Table 2. Comparison of the experimentally applied drying temperature with the estimated optimum drying temperature for 4 test batches (case study A) using the process control methodology.

		Estimated drying temperature based on predicted bulk density (°C)									
Batch	Used T_{drying} (°C)	M0	M1	M2	M3	M4	M5	M6	M7	M8	M9
T4	50	50	50	50	50	49	49	49	49	49	50
T8	70	76	75	75	74	73	73	72	72	73	73
TCP1	60	60	60	60	60	60	59	58	57	55	54
TCP2	60	61	58	57	56	56	56	55	54	53	53
		Estimated drying temperature based on predicted tapped density (°C)									
Batch	Used T_{drying} (°C)	M0	M1	M2	M3	M4	M5	M6	M7	M8	M9
T4	50	49	50	50	50	49	49	49	50	50	50
T8	70	73	73	72	71	70	69	69	69	70	70
TCP1	60	60	60	59	59	59	59	58	57	56	54
TCP2	60	60	57	56	56	56	56	55	54	54	53

Table 3. Comparison of the experimentally applied drying temperature with the estimated optimum drying temperature for 4 test batches (case study B) using the process control methodology.

		Estimated drying temperature based on predicted bulk density (°C)				
Batch	Used T_{drying} (°C)	M1	M2	M3	M4	M5
T1	50	52	52	51	53	54
T5a	70	67	68	62	64	63
T5b	70	69	71	67	72	71
T8	70	73	72	68	70	68
		Estimated drying temperature based on predicted tapped density (°C)				
Batch	Used T_{drying} (°C)	M1	M2	M3	M4	M5
T1	50	51	49	52	52	54
T5a	70	75	73	69	69	68
T5b	70	78	81	80	78	79
T8	70	77	79	74	73	71

Table 4. Use of the developed granulation feed-forward control strategy. Comparison of the predicted bulk density (BD) at the end of the spraying period using a drying temperature of 50°C, with the experimentally measured bulk density applying a drying temperature of 50°C (batch CS) and 67°C (batch CS adjusted a and b).

	Predicted BD (g mL^{-1})					Measured BD (g mL^{-1})	
Batch ID	M1	M2	M3	M4	M5	T_{drying} 50°C	T_{drying} 67°C
CS	0.5174	0.5136	0.5165	0.5119	0.5102	0.5161	
CS adjusted a	0.5233	0.5185	0.5248	0.5192	0.5197		0.4823
CS adjusted b	0.5173	0.5130	0.5172	0.5058	0.5044		0.4792

Table 5. Moisture content (MC) and standard deviation determined using Karl Fischer (KF) and predicted by the near infrared PLS calibration model for the design granulations performed in case study B.

DoE Batch	KF MC (%)	in-line NIR (%)	at-line NIR (%)
1	6.21 ± 0.23	7.69 ± 0.00	7.23 ± 0.12
2	7.13 ± 0.18	7.05 ± 0.02	7.19 ±0.04
3	7.28 ± 0.02	7.01 ± 0.04	7.22 ±0.07
4	6.87 ± 0.07	6.88 ± 0.01	6.81 ±0.03
5	7.01 ± 0.35	7.33 ± 0.02	7.36 ±0.06
6	7.69 ± 0.12	7.46 ± 0.04	7.31 ±0.06
7	7.21 ± 0.22	7.40 ± 0.04	7.25 ±0.10
8	7.23 ± 0.08	7.55 ± 0.03	6.51 ±0.04
9	6.72 ± 0.21	7.19 ± 0.02	7.13 ±0.04
10	7.38 ± 0.06	7.03 ± 0.08	7.56 ±0.05
11	7.17 ± 0.08	7.06 ± 0.00	7.15 ±0.04

Figure 1.

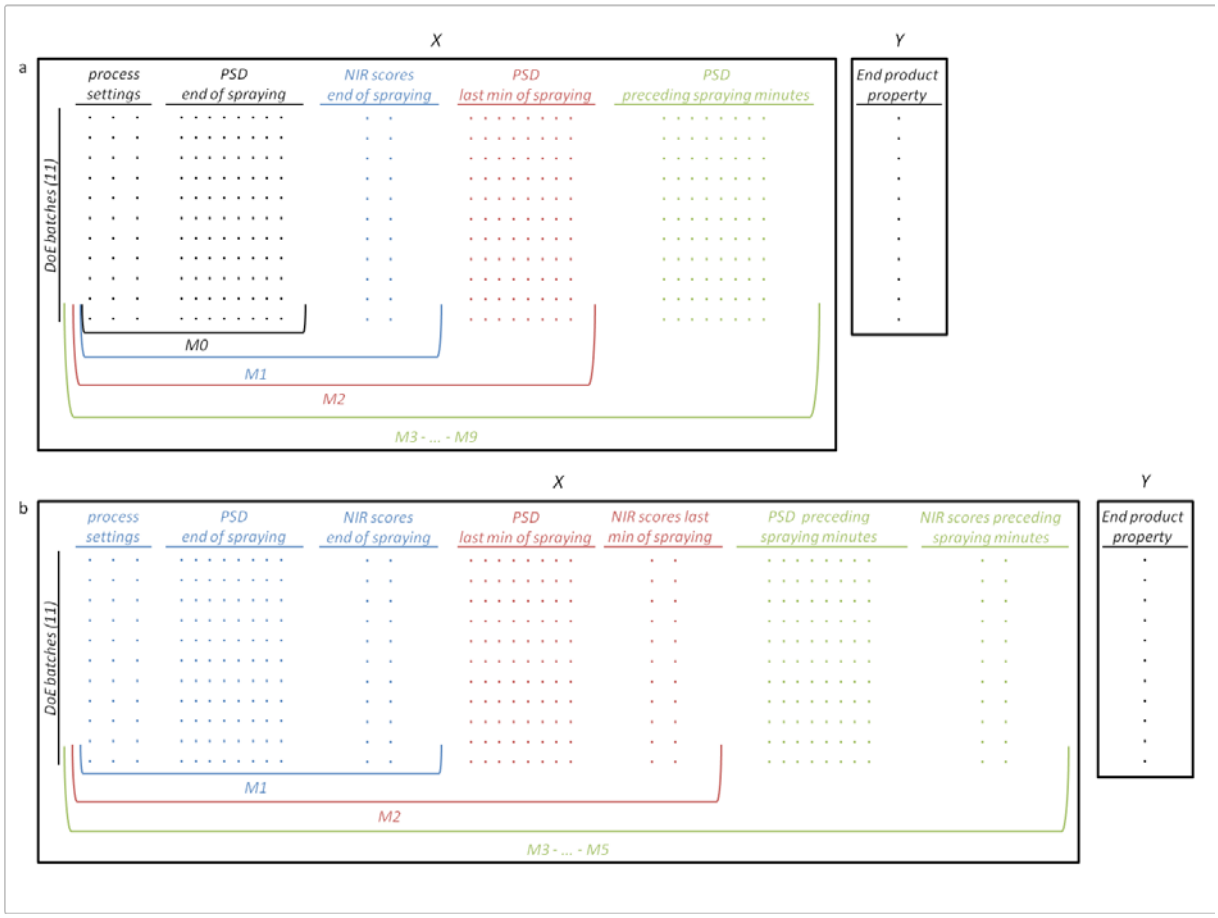
a
X
Y
process settings
PSD end of spraying
NIR scores end of spraying
PSD last min of spraying
PSD preceding spraying minutes
End product property
DoE batches (11)
M0
M1
M2
M3 - ... - M9
b
X
Y
process settings
PSD end of spraying
NIR scores end of spraying
PSD last min of spraying
NIR scores last min of spraying
PSD preceding spraying minutes
NIR scores preceding spraying minutes
End product property
DoE batches (11)
M1
M2
M3 - ... - M5

Figure 2.

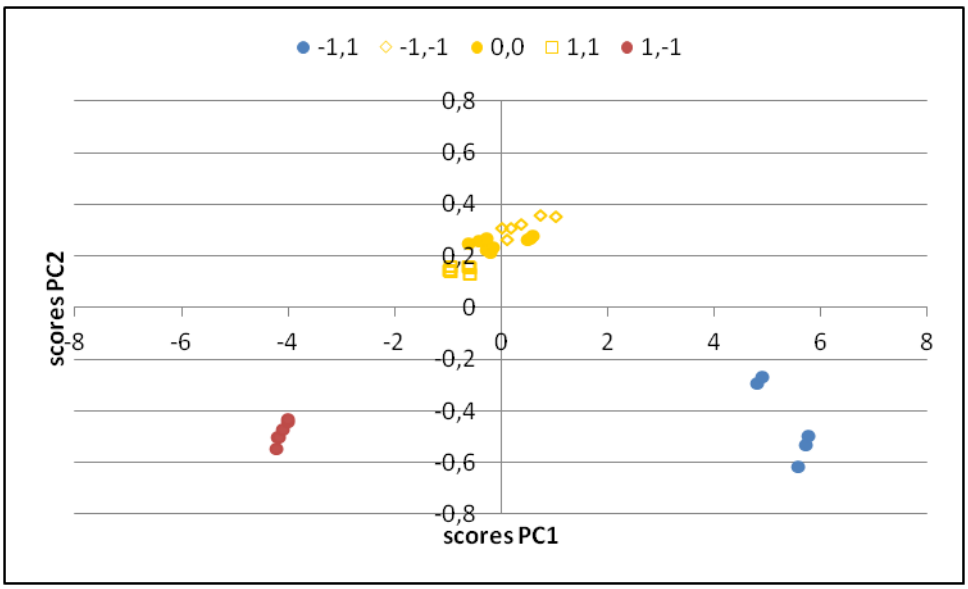
-1,1
-1,-1
0,0
1,1
1,-1
0,8
0,6
0,4
0,2
0
-0,2
-0,4
-0,6
-0,8
-8
-6
-4
-2
0
2
4
6
8
scores PC2
scores PC1

Figure 3.

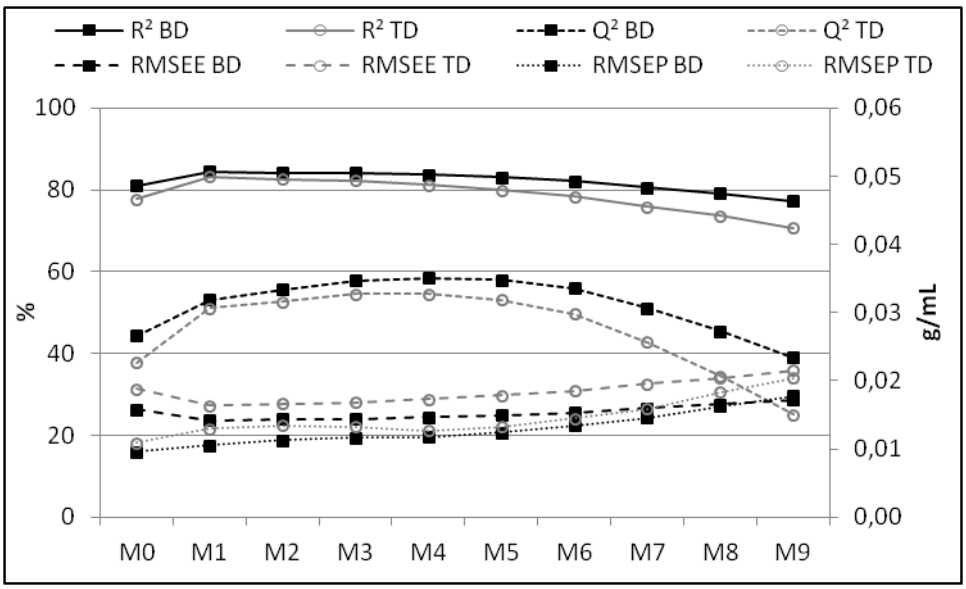
R² BD
R² TD
Q² BD
Q² TD
RMSEE BD
RMSEE TD
RMSEP BD
RMSEP TD
100
80
60
40
20
0
%
0,06
0,05
0,04
0,03
0,02
0,01
0,00
g/mL
M0
M1
M2
M3
M4
M5
M6
M7
M8
M9

Figure 4.

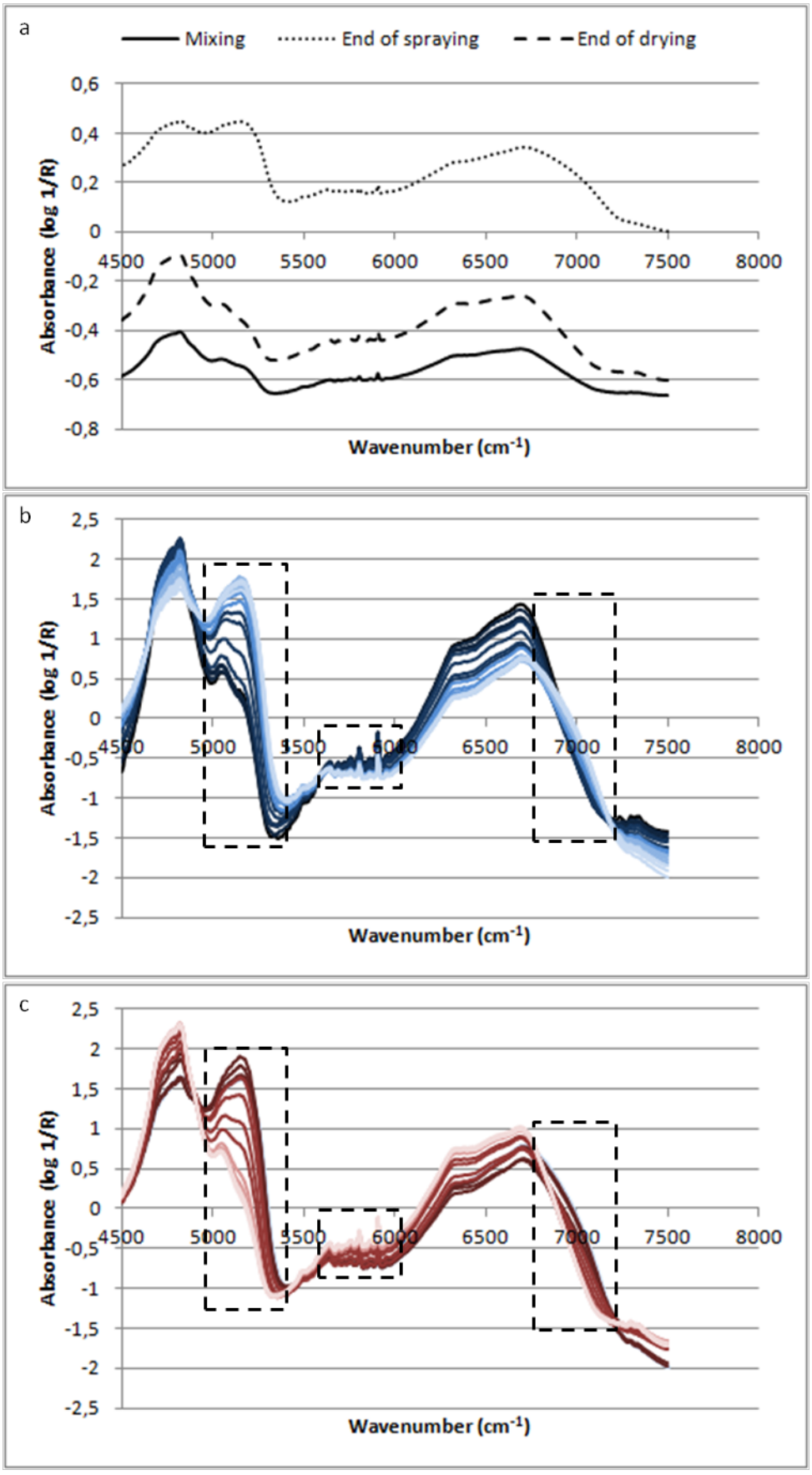
a
Mixing
End of spraying
End of drying
Absorbance (log 1/R)
Wavenumber (cm-1)
b
Absorbance (log 1/R)
Wavenumber (cm-1)
c
Absorbance (log 1/R)
Wavenumber (cm-1)

d

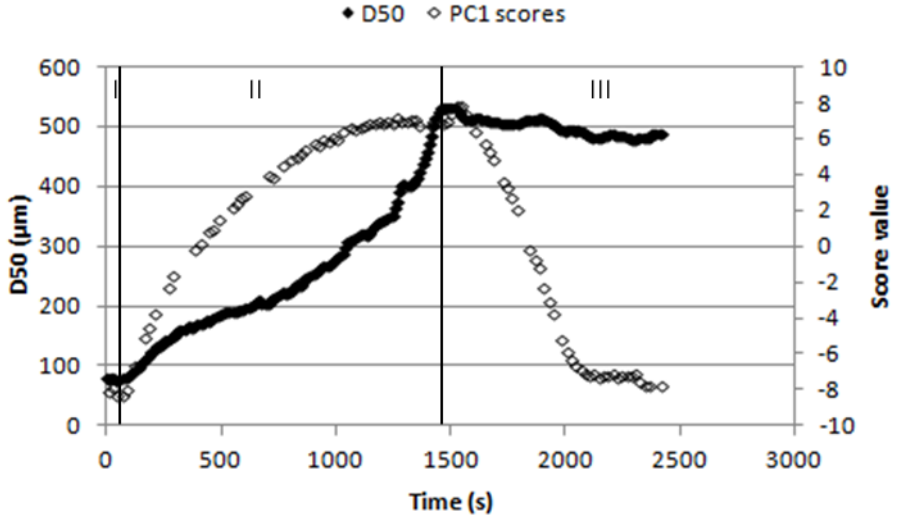
D50
PC1 scores
I
II
III
D50 (µm)
Score value
Time (s)
0
100
200
300
400
500
600
-10
-8
-6
-4
-2
0
2
4
6
8
10
0
500
1000
1500
2000
2500
3000

e

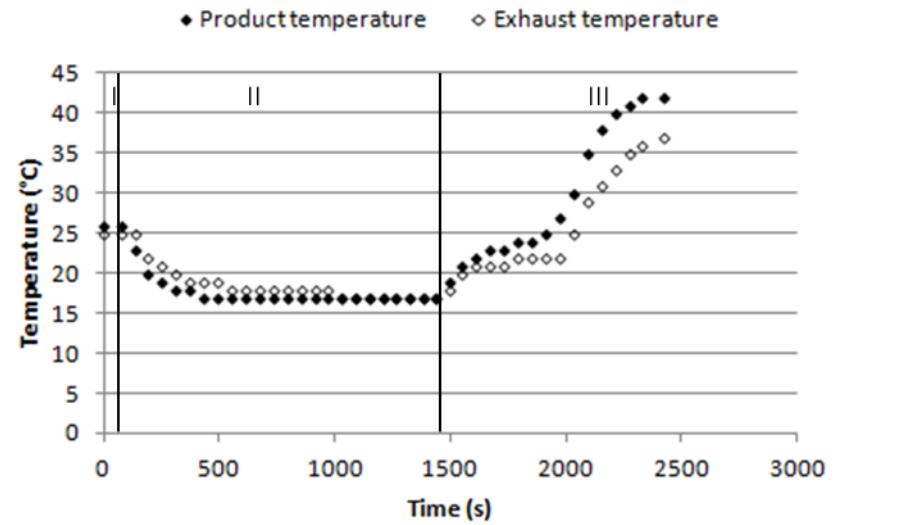
Product temperature
Exhaust temperature
I
II
III
Temperature (°C)
Time (s)
0
5
10
15
20
25
30
35
40
45
0
500
1000
1500
2000
2500
3000

Figure 5.

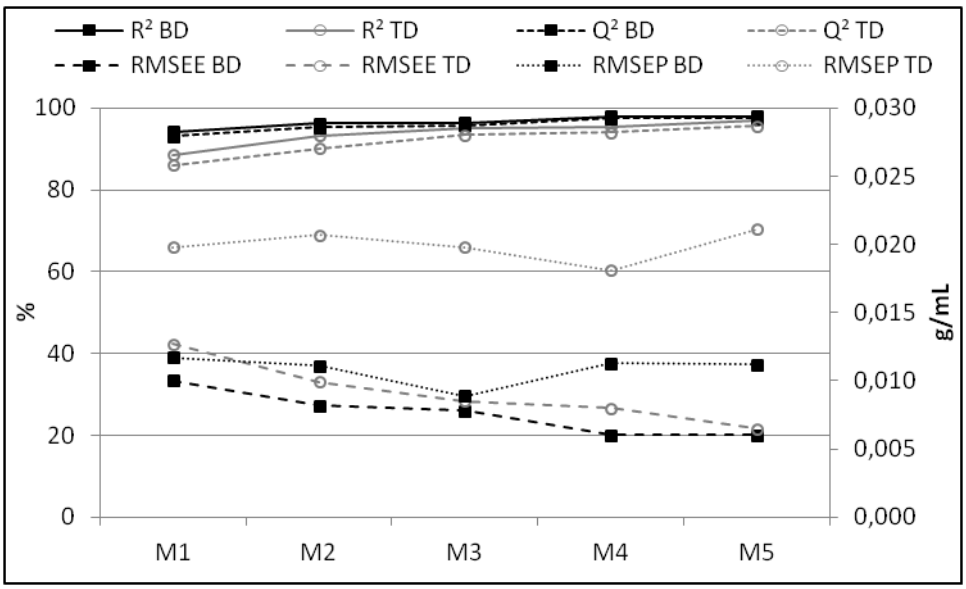
R² BD
R² TD
Q² BD
Q² TD
RMSEE BD
RMSEE TD
RMSEP BD
RMSEP TD
100
80
60
40
20
0
%
0,030
0,025
0,020
0,015
0,010
0,005
0,000
g/mL
M1
M2
M3
M4
M5

Figure S1.

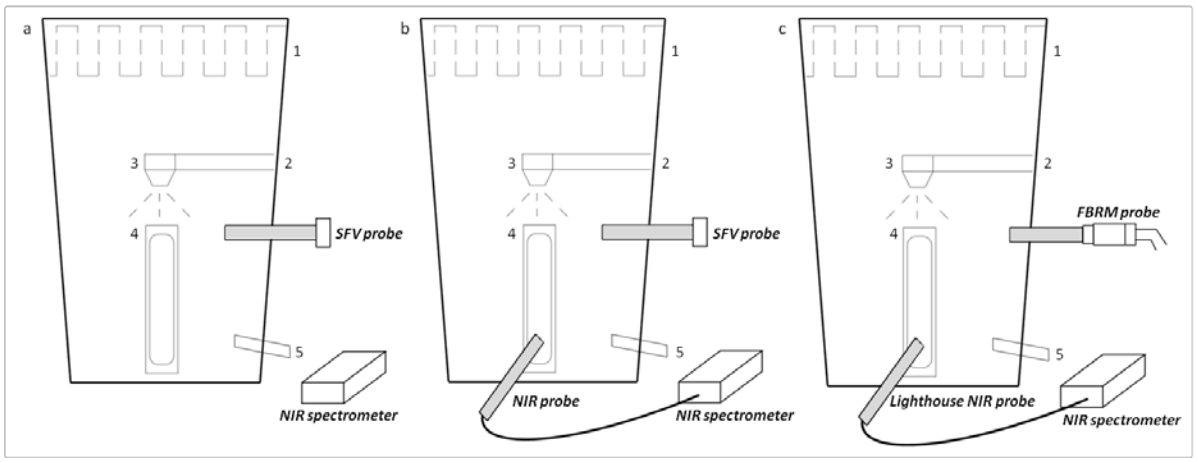
a
1
3
2
4
SFV probe
5
NIR spectrometer
b
1
3
2
4
SFV probe
5
NIR probe
NIR spectrometer
c
1
3
2
4
FBRM probe
5
Lighthouse NIR probe
NIR spectrometer

Figure S2.

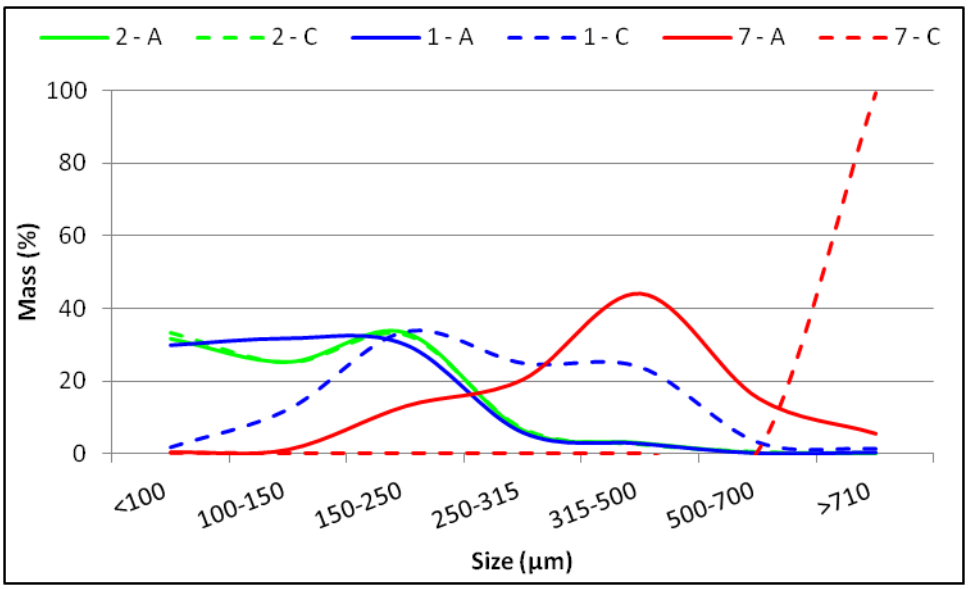
2 - A
2 - C
1 - A
1 - C
7 - A
7 - C
100
80
60
40
20
0
Mass (%)
<100
100-150
150-250
250-315
315-500
500-700
>710
Size (µm)

Figure S3.

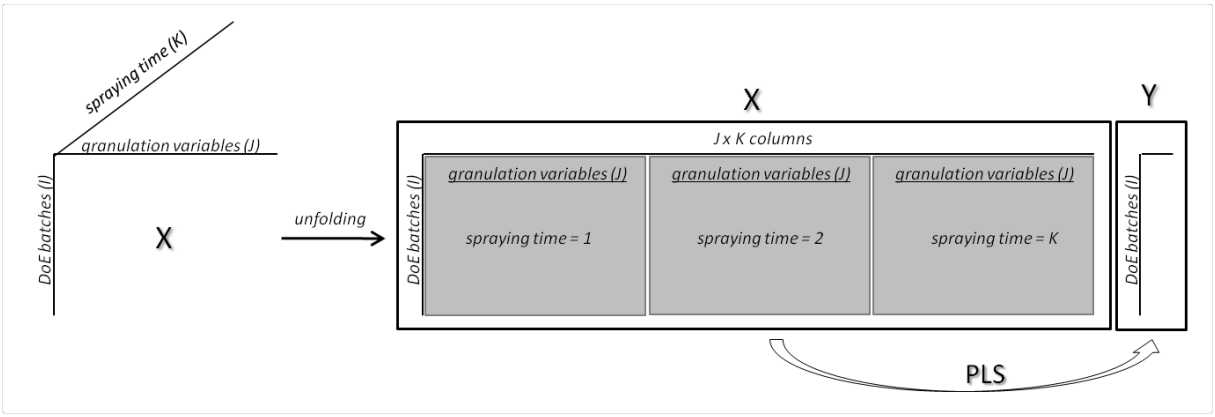
spraying time (K)
granulation variables (J)
DoE batches (I)
X
unfolding
X
Y
J x K columns
granulation variables (J)
granulation variables (J)
granulation variables (J)
spraying time = 1
spraying time = 2
spraying time = K
DoE batches (I)
DoE batches (I)
PLS

Figure S4.

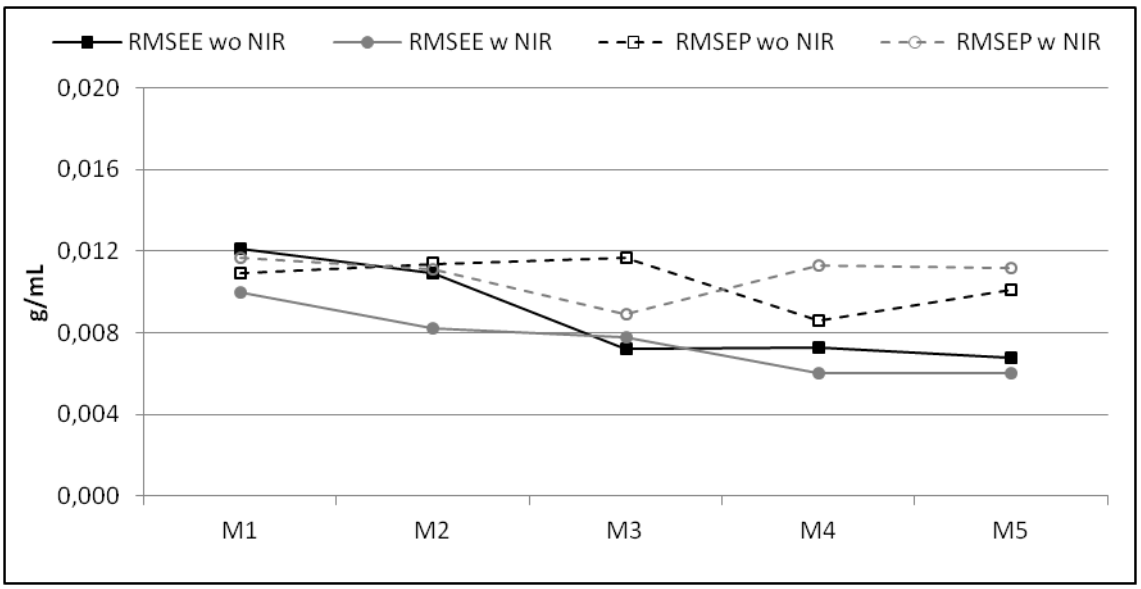
RMSEE wo NIR
RMSEE w NIR
RMSEP wo NIR
RMSEP w NIR
0,020
0,016
0,012
0,008
0,004
0,000
g/mL
M1
M2
M3
M4
M5